American Mineralogist, Volume 84, pages 1895–1901, 1999

Order-disorder kinetics in orthopyroxene with exsolution products

MICHELE ZEMA,[1,*] M. CHIARA DOMENEGHETTI,[2,†] AND VITTORIO TAZZOLI[1]

[1]Dipartimento di Scienze della Terra, Via Ferrata 1, 27100 Pavia, Italy
[2]CNR–Centro di Studio per la Cristallochimica e la Cristallografia, Dipartimento di Scienze della Terra, via Ferrata 1, 27100 Pavia, Italy

ABSTRACT

The equilibrium behavior and kinetics of the Fe-Mg intracrystalline exchange reaction in an orthopyroxene sample containing exsolution products were studied by X-ray diffraction (XRD). Isothermal annealing experiments were performed on an orthopyroxene crystal from the Johnstown diogenite, which shows coherent (100) augite lamellae and Guinier-Preston zones. The kinetic experiments were carried out at 700, 800, and 850 °C until Fe-Mg exchange equilibrium was reached. Oxygen fugacity was controlled by the WI buffer. Equilibrium conditions were also confirmed by "reversal" experiments. After each annealing run single-crystal XRD data were collected, and the orthopyroxene phase (*Pbca*) was refined after subtraction of the contribution of the exsolved *C*2/*c* phase to the observed structure factors. The fraction of augite was ~2%. The low values of the disordering rate constants K^+, calculated using Mueller's equation, and the surprisingly high value of the activation energy (102.3 kcal/mol) for the Fe-Mg disordering reaction are ascribed to the presence of exsolution products in the orthopyroxene. Exsolution products seem not to affect the equilibrium behavior.

INTRODUCTION

In orthopyroxene, Fe^{2+} and Mg fractionate between the two non-equivalent crystallographic sites M1 and M2 with Fe^{2+} preferring the M2 site and Mg the M1 site. This non-convergent ordering-disordering process can be described by the following chemical exchange reaction:

$$Fe^{2+}(M2) + Mg(M1) \underset{\text{ordering}}{\overset{\text{disordering}}{\rightleftharpoons}} Fe^{2+}(M1) + Mg(M2) \quad (1)$$

The Fe^{2+}-Mg site distribution is strongly dependent on temperature and composition.

Interest in both the equilibrium behavior and the kinetics of the exchange process is mainly due to the possibility of using orthopyroxenes as indicators of the thermal history of igneous and metamorphic rocks (Ganguly 1982). A geospeedometer based on the Fe-Mg exchange in orthopyroxene was recently applied to meteorites as well (Ganguly et al. 1994; Molin et al. 1994; Zema et al. 1996; Kroll et al. 1997; Zema et al. 1997), to constrain their evolutionary histories through the calculation of their cooling rates.

The temperature dependence of the equilibrium Fe-Mg fractionation has been the subject of various studies carried out on both natural and synthetic orthopyroxenes (Saxena and Ghose 1971; Seifert 1983; Molin et al. 1991; Yang and Ghose 1994). Empirical equations that express the equilibrium distribution coefficient K_D as a function of temperature were developed to allow the calculation of the closure temperatures for the Fe-Mg exchange from the quenched ordering state of an orthopyroxene crystal (Ganguly and Domeneghetti 1996; Kroll et al. 1997). Recently Stimpfl et al. (1999) obtained the following equation:

$$\ln K_D = -2557(\pm 49)/T + 0.547(\pm 0.048) \quad (2)$$

where temperature T is in Kelvin, by statistical regression of $\ln K_D$ vs. X_{Fe} and T data selected from the literature according to the criteria suggested by Kroll et al. (1997). This equation is valid in the compositional range $Fs_{19} - Fs_{75}$ (Fs is Ferrosilite), thus reinforcing the conclusion of Ganguly and Domeneghetti (1996) that there is no significant compositional dependence of K_D over a wide X_{Fe} range.

Determination of closure temperatures from the K_D values using the above expression represents an important step in constraining the thermal history of a crystal because it can give an initial indication of the rate of the cooling process. More specific information, however, comes from the kinetic study of the Fe-Mg exchange reaction, which can give a quantitative evaluation of the cooling rate. For this purpose, Mueller's (1967, 1969) approach, as developed by Ganguly (1982), turned out to be very useful. Mueller treated the Fe-Mg exchange in orthopyroxene as a homogeneous chemical reaction following second-order kinetics and developed a simple expression, which is valid for a binary system, to describe the variation with time of the ordering degree under isothermal conditions.

*Present address: Centro Grandi Strumenti, Università di Pavia, Via Bassi 21, 27100 Pavia, Italy
†E-mail: Domeneghetti@crystal.unipv.it

0003-004X/99/1112–1895$05.00

Based on this theory, the kinetics of the cation disordering in orthopyroxene was studied both by Mössbauer spectroscopy (Besancon 1981; Anovitz et al. 1988) and by single-crystal XRD (Saxena et al. 1987; Saxena et al. 1989; Skogby 1992; Sykes-Nord and Molin 1993). All these experimental studies confirmed Mueller's assumption that the kinetics of the exchange process follows a second-order rate law. By least squares fitting of a selected set of data taken from the literature, Ganguly and Tazzoli (1994) obtained an optimized expression for the disordering rate constant $K^+(\text{min}^{-1})$ as a function of temperature and X_{Fe}, as follows:

$$\ln K^+ = (26.2 + 6.0\ X_{Fe}) - 62767/(RT) \quad (3)$$

where R is the gas constant, thus finding an averaged value of the activation energy of the exchange process of 62.767(±2.223) kcal/mol within the compositional range $X_{Fe} = 0.10$–0.50. Kroll et al. (1997) also derived coefficients for the dependence of K^+ on T and X_{Fe} from published and their own data. They obtained the following equation from 27 rate constants measured on orthopyroxenes with composition $0 < X_{Fe} < 0.55$:

$$\ln K^+ = 28.12(80) - [32241(752) - 6012(647)X_{Fe}^2]/(RT). \quad (4)$$

This equation, applied to a sample with $X_{Fe} = 0.255$ as in Johnstown orthopyroxene, yields an activation energy of 63.3 kcal/mol, very close to the value of Equation 3.

All the experimental data used in the above studies were obtained from samples in which the presence of exsolution products had not been revealed. Such products, however, are commonly present in orthopyroxenes which contain some Ca and which have undergone very slow cooling. The aim here is to investigate whether these exsolution products actually affect the kinetics and/or the equilibrium behavior of the Fe-Mg exchange reaction in orthopyroxene. An orthopyroxene single crystal (JS15) from the Johnstown diogenite, containing both (100) exsolved augite lamellae and Guinier-Preston (GP) zones, was isothermally heated at different temperatures between 700 and 850 °C. To constrain the activation energy and the equilibrium conditions, data obtained on another single crystal (JS16) from the same Johnstown fragment (Zema et al. 1999) were also used in the calculations.

Experimental methods

Sample

The Johnstown diogenite is a brecciated orthopyroxenite containing coarse-grained clasts of cumulate origin. Olivine, chromite, plagioclase, troilite, silica, and metals are also present as minor phases (Floran et al. 1981). The orthopyroxene from the Johnstown diogenite has a very homogeneous major element composition, $Wo_3En_{74}Fs_{23}$, which is very close to the mean composition of meteoritic diogenites (Fredriksson 1976; Mittlefehldt 1994). It contains ~100 Å thick coherent augite lamellae and Guinier-Preston zones (Mori and Takeda 1981), which should indicate rapid cooling at high magmatic temperatures and slow cooling at very low temperatures (Molin et al. 1991).

The experimental work was carried out on the orthopyroxene single crystal JS15, measuring 0.33 mm × 0.36 mm × 0.40 mm. Under crossed polarizers it appeared to be homogeneous and free of inclusions. The diffraction profiles were narrow and the cell parameters very similar to those of sample JS16 (Zema et al. 1999). Like JS16, crystal JS15 showed some (0*kl*) reflections with $k = 2n + 1$ and $l = 4n + 2$ which violate the extinction conditions of the *Pbca* space group of the orthopyroxene, but are consistent with an exsolved augite phase (Domeneghetti et al. 1995).

Annealing experiments

A series of isothermal heating runs were performed at 700, 800, and 850 °C until equilibrium was reached at each temperature. Equilibrium conditions at 700, 750, and 800 °C were confirmed by reversal experiments, i.e., crystal JS15 was disordered at 700 °C until equilibrium was attained, then disordered at 800 °C and re-ordered at 700 °C. Finally, it was disordered at 850 °C and re-ordered at 800 and at 750 °C. The sequence of the heating runs is reported in Table 1. The data obtained from crystal JS16 (Zema et al. 1999) were used for the disordering process at 750 °C.

The annealing experiments were performed in a vertical, temperature-controlled [± 3 °C, Pt/(Pt-Rh) thermocouple] furnace. The experiments were carried out in silica tubes that were sealed after a preliminary alternate flushing with Ar and evacuation to reduce the oxygen concentration. A wüstite-iron (WI) buffer was used in addition to control the f_{O_2}. The crystal and the buffer were put into the tubes in two separate small Pt crucibles so as to avoid contact. The presence of both iron and wüstite, in a different ratio compared to that in the original powder, was verified at the end of each run by X-ray powder diffraction. The crystal was quenched by dropping the tubes into cold water.

X-ray single crystal diffraction

The quenched Fe-Mg ordering degrees of both the untreated and the annealed crystal were determined from single-crystal XRD. Intensity data were collected on a Philips PW 1100 four-circle automated diffractometer with graphite monochromated Mo$K\alpha$ radiation ($\lambda = 0.71073$ Å, 60 kV, 25 mA). The unit-cell parameters were determined using a locally improved version (Cannillo et al. 1983) of the Philips LAT routine on 50–60 reflections and are reported in Table 2. Net X-ray diffraction intensities were obtained by measuring step-scan profiles and analyzing them by the Lehman and Larsen (1974) σ_I / I method, as modified by Blessing et al. (1974). The equivalent pairs *hkl*, $\bar{h}kl$ were measured up to $\theta = 30°$ using the ω-scan mode. The intensities were corrected for absorption using the ψ scan method of North et al. (1968).

Structure refinements were carried out using the procedure described by Domeneghetti et al. (1996) which allows the refinement of a *Pbca* phase coexisting with a *C*2/*c* exsolved phase. The estimated fraction of the *C*2/*c* phase measured in the un-

Table 1. Sequence of annealing experiments carried out on sample JS15

Process (°C)	Total time	No. of steps
Disordering at 700	500 h	5
Disordering at 800	2 h	6
Ordering at 700 (reversal)	500 h	1
Disordering at 850	80 min	7
Ordering at 800 (reversal)	2 h	1
Ordering at 750 (reversal)	24 h	1

treated crystal JS15 and after each heating run is reported in Table 2. It is worth noting that this fraction (about 2.0%) remained practically constant over all the annealing experiments. This value is in perfect agreement with that estimated by TEM analysis on sample JS16 (Camara, personal communication). The observed structure factors, "cleaned up" from the contribution of the monoclinic phase, were used for further refinement of the *Pbca* phase. This last refinement, based on F_o^2, was carried out by full-matrix least-squares using SHELXL-93 (Sheldrick 1993). The values of equivalent pairs were averaged and the resulting discrepancy factors $R_{int} = \sum \left| F_o^2 - \overline{F}_o^2 \right| / \sum F_o^2$ are reported in Table 2. R_{int} decreased by about 0.5 after subtracting the contribution of the exsolved phase. No chemical constraints were used in the refinements. The atomic scattering curves were taken from the *International Tables for X-ray Crystallography* (Ibers and Hamilton 1974) and from Tokonami (1965). Complete ionization for Mg and Fe in M1 and M2 sites was adopted following Rossi et al. (1983), 2.0^+ for Si in SiA and SiB sites and 1.5^- for O. The extinction correction of Coppens and Hamilton (1970) was applied. In addition to scale factor and isotropic extinction coefficient, 30 atomic positions, anisotropic displacement parameters and site occupancies of M1 and M2 sites were refined, varying all parameters simultaneously. No correlation >0.60 was observed, and the final difference-Fourier maps were featureless. For all runs the number of total and unique reflections I_{tot} and I, respectively, was ~2800 and ~1235. The conventional discrepancy indices R_1, based on $F_o^2 > 2\sigma(F_o^2)$ and R_{all}, based on all the F_o^2, as well as the goodness of fit (S) and refinement data are reported in Table 2. Interatomic distances, final atomic parameters and observed and calculated structure factors are available from the authors.

Site populations were calculated using the refined structural parameters and the results of electron microprobe analysis. To preserve it for further studies, chemical analysis was not performed on the crystal JS15, but are from similar samples (Table 3). The refined structural parameters and the microprobe data were treated by a minimization program based on the MINUIT library (James and Roos 1975). Procedural details are in Zema et al. (1997). Here, the sum of the mean atomic numbers of M1 and M2, averaged on all runs, was introduced as a further constraint in the minimization. The atomic fractions of Fe and Mg, which define the ordering state of the crystal, are reported in Table 4.

TABLE 2a. Cell parameters and information on data collection and structure refinements before and after annealing runs at 700 °C

Annealing time	*a* (Å)	*b* (Å)	*c* (Å)	*V* (Å^3)	R_{int}	Fraction of *C2/c* phase (%)	R_1 (%)	R_{all} (%)	*S*	m.a.n.* (M1)	m.a.n.* (M2)	m.a.n.* (M1 + M2)
Untreated	18.280(5)	8.864(2)	5.204(2)	843.2	2.93	1.5	2.13	3.35	1.210	12.74(3)	18.90(3)	31.64(4)
15h	18.287(4)	8.868(2)	5.205(2)	844.1	2.71	1.9	2.98	3.88	1.185	12.90(5)	18.67(5)	31.57(7)
60h	18.288(4)	8.869(2)	5.206(2)	844.5	1.98	1.8	2.14	3.23	1.192	13.25(3)	18.30(4)	31.55(5)
120h	18.290(6)	8.869(2)	5.207(3)	844.6	1.82	1.9	2.62	3.70	1.217	13.36(4)	18.26(5)	31.62(6)
250h	18.289(5)	8.868(2)	5.206(2)	844.4	2.33	1.4	2.33	3.72	1.263	13.42(4)	18.23(5)	31.65(7)
500h	18.285(7)	8.866(3)	5.203(3)	843.5	2.93	1.7	2.36	3.81	1.280	13.39(4)	18.17(4)	31.56(6)
Reversal†	18.282(5)	8.865(2)	5.204(2)	843.5	2.00	2.2	2.49	3.71	1.264	13.45(4)	18.18(5)	31.63(6)

Note: Standard deviations are given in parentheses; $R_{int} = \Sigma |F_o^2 - F_o^2(\text{mean})| / \Sigma [F_o^2]$; $R_1 = \Sigma ||F_o| - |F_c|| / \Sigma |F_o|$; $S = [\Sigma [w(F_o^2 - F_c^2)^2] / (n - p)]^{0.5}$, where n is the number of reflections and p is the total number of parameters refined.
* m.a.n. is the mean atomic number.
† Starting point: equilibrium condition at 800 °C; annealing time: 500h.

TABLE 2b. Cell parameters and information on data collection and structure refinements after annealing runs at 800 °C and after the reversal experiment at 750 °C

Annealing time	*a* (Å)	*b* (Å)	*c* (Å)	*V* (Å^3)	R_{int}	Fraction of *C2/c* phase (%)	R_1 (%)	R_{all} (%)	*S*	m.a.n.* (M1)	m.a.n.* (M2)	m.a.n.* (M1 + M2)
7 min	18.280(5)	8.865(2)	5.204(2)	843.2	2.41	1.9	2.50	3.58	1.212	13.48(4)	18.13(4)	31.61(6)
20 min	18.286(5)	8.867(3)	5.206(3)	844.0	2.48	2.0	2.36	3.38	1.186	13.63(4)	18.06(4)	31.69(6)
31 min	18.281(4)	8.864(2)	5.202(2)	842.9	2.16	1.9	2.24	3.86	1.176	13.53(4)	18.00(4)	31.53(6)
40 min	18.287(8)	8.869(3)	5.206(2)	844.2	2.15	1.9	2.61	3.61	1.231	13.62(4)	18.00(4)	31.62(6)
121 min	18.284(8)	8.867(2)	5.204(2)	843.7	2.90	2.2	2.67	3.96	1.311	13.64(5)	17.98(5)	31.62(7)
Reversal*	18.286(4)	8.867(2)	5.205(2)	843.9	2.30	1.7	2.11	3.69	1.199	13.65(3)	17.94(4)	31.59(5)
at 750 °C†	18.288(4)	8.870(2)	5.206(1)	844.5	1.86	2.1	2.36	3.19	1.216	13.46(4)	18.02(4)	31.48(6)

* Starting point: equilibrium condition at 850 °C; annealing time: 120 min.
† Starting point: equilibrium condition at 800 °C reached after the reversal experiment; annealing time: 1440 min.

TABLE 2c. Cell parameters and information on data collection and structure refinements after annealing runs at 850 °C

Annealing time	*a* (Å)	*b* (Å)	*c* (Å)	*V*(Å^3)	R_{int}	Fraction of *C2/c* phase (%)	R_1 (%)	R_{all} (%)	*S*	m.a.n.* (M1)	m.a.n.* (M2)	m.a.n.* (M1 + M2)
1 min	18.290(4)	8.869(2)	5.206(2)	844.6	1.80	2.1	2.36	3.09	1.201	13.54(4)	18.02(4)	31.56(6)
3 min	18.290(4)	8.869(2)	5.206(1)	844.4	2.43	1.5	2.11	3.50	1.321	13.58(4)	17.94(4)	31.52(6)
6 min	18.290(4)	8.870(2)	5.206(1)	844.7	1.97	2.1	2.36	3.29	1.204	13.62(4)	17.91(4)	31.53(6)
15 min	18.293(5)	8.873(2)	5.207(2)	845.2	1.91	2.2	2.32	3.15	1.247	13.72(4)	17.86(4)	31.58(6)
25 min	18.289(6)	8.870(3)	5.206(2)	844.5	2.10	1.9	2.14	2.84	1.192	13.65(4)	17.80(4)	31.45(6)
35 min	18.286(5)	8.867(3)	5.205(2)	844.0	2.01	2.0	2.47	3.46	1.262	13.70(4)	17.85(4)	31.55(6)
80 min	18.287(5)	8.868(2)	5.205(2)	844.1	2.25	1.6	2.23	3.55	1.172	13.70(3)	17.83(4)	31.53(5)

TABLE 3. Chemical composition of the orthopyroxene from Johnstown diogenite

Oxide (wt%)		Atoms per formula unit*	
SiO_2	54.13(15)	Si	1.963(3)
Al_2O_3	1.09(4)	Al	0.046(3)
FeO	15.10(11)	Fe^{2+}	0.458(6)
MgO	26.60(12)	Mg	1.437(4)
MnO	0.47(2)	Mn	0.014(1)
TiO_2	0.10(1)	Ti	0.003(1)
Cr_2O_3	0.82(3)	Cr	0.024(1)
CaO	1.40(7)	Ca	0.054(3)
Na_2O	0.01(1)	Na	0.001(1)
Sum	99.48	Sum	4.000

Notes: Standard deviations are given in parentheses; average of 200 electron microprobe spot analyses of several crystals (Zema et al. 1997).
* Based on six O atoms.

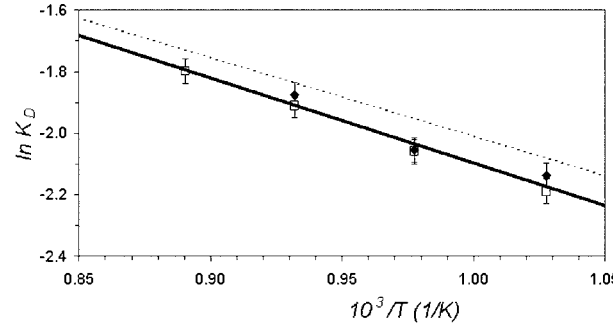

FIGURE 1. The ln K_D vs. $1/T$(K) plot for the orthopyroxene from Johnstown (thicker solid line). Empty squares refer to disordering and filled diamonds to ordering experiments. Dashed line is the calibration of Stimpfl et al. (1999).

RESULTS AND DISCUSSION

The equilibrium conditions reached at each temperature were defined using the equilibrium distribution coefficient K_D:

$$K_D = \frac{X_{Fe}^{M1}\left(1 - X_{Fe}^{M2}\right)}{X_{Fe}^{M2}\left(1 - X_{Fe}^{M1}\right)} \quad (5)$$

where X_{Fe}^{M1} is the atomic fraction of Fe^*, i.e., $Fe^*/(Fe^* + Mg)$ at the M1 site, and similarly for X_{Fe}^{M2} with $Fe^* = Fe^{2+} + Mn$. The values for sample JS15 are in Table 4. These data have been treated together with those obtained on sample JS16 (Zema et al. 1999). The least squares fit of the two data sets yields

$$\ln K_D = -2766(\pm 210)/T + 0.669(\pm 0.20) \ (R^2 = 0.97) \quad (6)$$

where temperature T is Kelvin. This regression straight line (Fig. 1) is in good agreement with that of Stimpfl et al. (1999), the differences being within the standard deviations, thus confirming that the equilibrium behavior of orthopyroxene is not affected by the presence of exsolution products.

The analysis of the kinetic data was performed using Mueller's (1969) equation

TABLE 4a. Atomic fractions in M1 and M2 sites and K_D values be fore and after annealing runs at 700 °C

	Mg(M1)	Fe*(M1)	X_{Fe}^{M1}	Mg(M2)	Fe*(M2)	X_{Fe}^{M2}	K_D
Untreated	0.9372(23)	0.0291	0.0301	0.4840(23)	0.4615	0.4881	0.0326(29)
15h	0.9251(36)	0.0413	0.0427	0.4998(38)	0.4458	0.4714	0.0501(49)
60h	0.8994(25)	0.0668	0.0691	0.5258(26)	0.4198	0.4440	0.0930(41)
120h	0.8929(32)	0.0734	0.0760	0.5304(33)	0.4152	0.4391	0.1050(55)
250h	0.8890(32)	0.0773	0.0800	0.5333(34)	0.4123	0.4360	0.1125(56)
500h	0.8899(30)	0.0764	0.0791	0.5353(30)	0.4103	0.4339	0.1120(53)
Reversal	0.8866(31)	0.0797	0.0825	0.5364(33)	0.4092	0.4327	0.1178(56)

Note: Standard deviations are in parentheses; $Fe^* = Fe + Mn$.

$$X_{Fe}^{M1} = \frac{(Fe^*)_{M1}}{(Fe^* + Mg)_{M1}}; X_{Fe}^{M2} = \frac{(Fe^*)_{M2}}{(Fe^* + Mg)_{M2}}; K_D = \frac{X_{Fe}^{M1}(1 - X_{Fe}^{M2})}{X_{Fe}^{M2}(1 - X_{Fe}^{M1})}$$

TABLE 4b. Atomic fractions in M1 and M2 sites and K_D values after annealing runs at 800 °C and after the reversal experiment at 750 °C

	Mg(M1)	Fe*(M1)	X_{Fe}^{M1}	Mg(M2)	Fe*(M2)	X_{Fe}^{M2}	K_D
7 min	0.8843(31)	0.0820	0.0849	0.5390(32)	0.4615	0.4299	0.1230(56)
20 min	0.8750(28)	0.0913	0.0945	0.5455(30)	0.4458	0.4231	0.1423(54)
31 min	0.8793(30)	0.0870	0.0900	0.5469(30)	0.4198	0.4216	0.1357(57)
40 min	0.8745(30)	0.0918	0.0950	0.5485(32)	0.4152	0.4199	0.1450(59)
121 min	0.8734(35)	0.0929	0.0961	0.5502(36)	0.4123	0.4181	0.1480(69)
Reversal	0.8713(25)	0.0950	0.0983	0.5524(26)	0.4092	0.4158	0.1532(50)
Reversal at 750 °C	0.8829(28)	0.0833	0.0862	0.5447(29)	0.4009	0.4240	0.1282(52)

TABLE 4c. Atomic fractions in M1 and M2 sites and K_D values after annealing runs at 850 °C

	Mg(M1)	Fe*(M1)	X_{Fe}^{M1}	Mg(M2)	Fe*(M2)	X_{Fe}^{M2}	K_D
1 min	0.8787(28)	0.0876	0.0907	0.5461(29)	0.3995	0.4225	0.1363(53)
3 min	0.8752(28)	0.0912	0.0944	0.5511(28)	0.3944	0.4171	0.1456(55)
6 min	0.8728(29)	0.0935	0.0968	0.5534(30)	0.3923	0.4148	0.1511(58)
15 min	0.8665(26)	0.0997	0.1032	0.5579(29)	0.3878	0.4101	0.1655(60)
25 min	0.8687(26)	0.0977	0.1011	0.5599(27)	0.3856	0.4078	0.1633(55)
35 min	0.8675(32)	0.0988	0.1022	0.5580(27)	0.3876	0.4099	0.1640(66)
80 min	0.8671(25)	0.0992	0.1027	0.5591(26)	0.3866	0.4087	0.1655(53)

$$-C_0K^+\Delta t = \frac{1}{(b^2-4ac)^{1/2}}\ln\left|\frac{(b^2-4ac)^{1/2}-[2aX_{Fe}^{M2}+b]}{(b^2-4ac)^{1/2}+[2aX_{Fe}^{M2}+b]}\right|_{X_{Fe}^{M2}(t_0)}^{X_{Fe}^{M2}(t)} \quad (7)$$

where a, b, and c depend on the composition of the crystal and on the equilibrium distribution coefficient K_D (see Table 4). C_0 is the total number of sites involved in the exchange process and it is usually included in the disordering rate constant K^+. The atomic fraction X_{Fe}^{M2} was then chosen to define the Fe-Mg ordering degree of the crystal. If Equation 7 is applicable, the plot of the quantity L

$$L = \ln\left|\frac{(b^2-4ac)^{1/2}-[2aX_{Fe}^{M2}+b]}{(b^2-4ac)^{1/2}+[2aX_{Fe}^{M2}+b]}\right|_{X_{Fe}^{M2}(t_0)}^{X_{Fe}^{M2}(t)} \quad (8)$$

vs. Δt gives a straight line with slope $-C_0K^+(b^2-4ac)^{1/2}$ from which the disordering rate constant C_0K^+ at a fixed temperature can be determined.

Very good linear fits of L vs. Δt were obtained for all temperatures (Fig. 2). The relevant disordering rate constants C_0K^+, as well as details of the calculations are reported in Table 5.

The close fit between the theoretical curves calculated using these C_0K^+ values in Mueller's equation and the experimental data points (Fig. 3) confirms that the Fe-Mg exchange reaction in orthopyroxene actually follows second-order kinetics and that the measured ordering states are highly reliable.

TABLE 5. Disordering rate constants and details of the calculations

T (°C)	C_0K^+	R^2 test	No. of points in the regression
700	$1.38\cdot10^{-4}$/min	0.9990	2
750*	$1.16\cdot10^{-3}$/min	0.996	5
800	0.0160/min	0.990	4
850	0.1505/min	0.94	2

* From Zema et al. (1999).

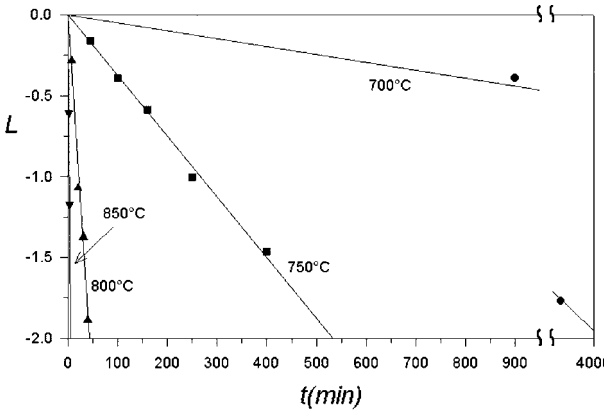

FIGURE 2. The L vs. Δt plot for the calculation of the disordering rate constants C_0K^+ at each temperature. The line for disordering experiments at 750 °C is from Zema et al. (1999). The point after the break on the x axis pertains to the 700 °C series.

The Arrhenius relation

$$\ln K^+ = \ln K_0 - Q/(RT) = 43.9(\pm2.3) - 102.3(\pm2.4)/(RT) \quad (R^2 = 0.996) \quad (9)$$

plotted in Figure 4 shows that, in the range of the temperatures investigated, the disordering rate constants of the Fe-Mg exchange reaction are always lower than those predicted by Equations 3 and 4 and the activation energy is much larger (102.3 kcal/mol rather than ~63 kcal/mol). Such a large activation energy for the exchange reaction has not been measured in the previous kinetic studies, performed on orthopyroxene crystals in which the presence of exsolution products had not been revealed. Because in XRD analysis the presence of (100) exsolved augite lamellae in a crystal is immediately shown by violations of *Pbca* extinction conditions, even if a preliminary check by TEM is not carried out, one can reasonably presume that

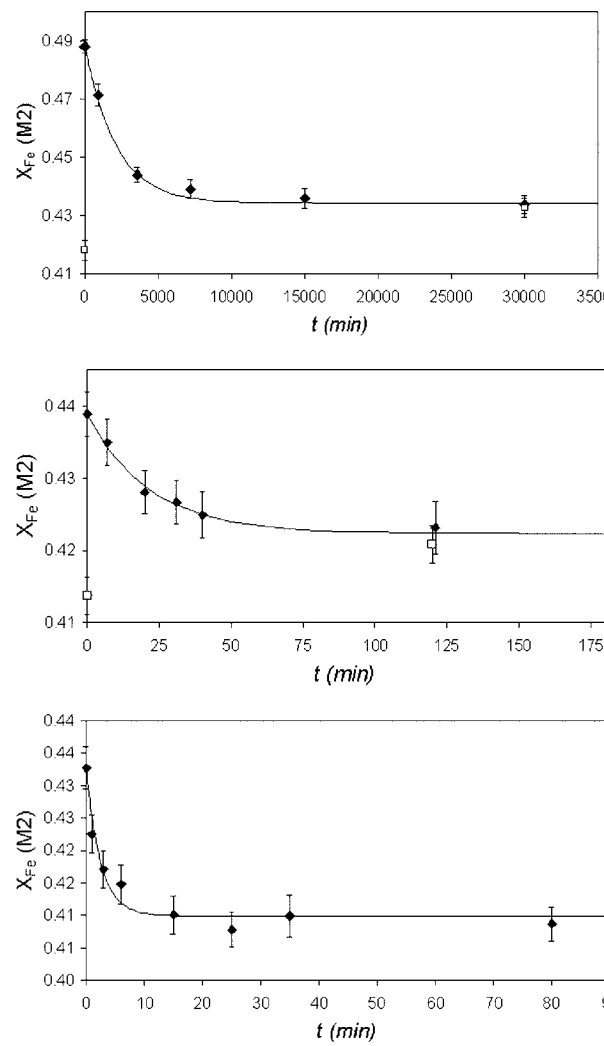

FIGURE 3. Experimental points superimposed on the theoretical curves calculated by Mueller's equation. Empty symbols represent reversal experiments. **Top** = 700 °C annealing; **middle** = 800 °C; **bottom** = 850 °C.

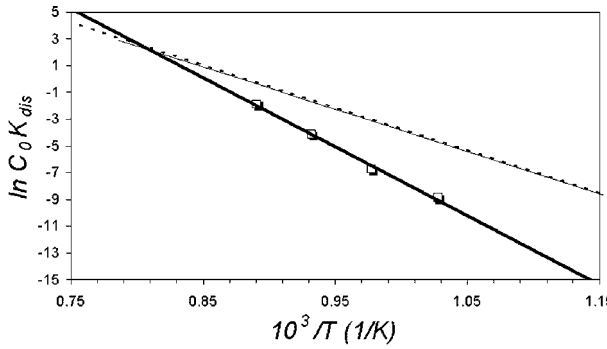

FIGURE 4. Arrhenius plot ln K = ln K^{+} – Q/(RT) which yields an activation energy of 102.3 kcal/mol for the Fe-Mg exchange process. Thin line = results from Ganguly and Tazzoli (1994). Dashed line = from Kroll et al. (1997). Thick line = this work.

orthopyroxene crystals used in those studies were really free of lamellae. For this reason, the slower kinetics measured on the Johnstown sample can be ascribed to the presence of exsolution products through a mechanism that, at present, is still unclear. The kinetic results here may have important implications in constraining the thermal history of the host rocks as cooling rates are retrieved from kinetic constants of the ordering–disordering process in orthopyroxene. If the exsolution products are responsible for a high activation energy, it is crucial to know if the ordering process in a slowly cooled Ca-rich sample took place before or after the exsolution process. This is because, in the first case, the kinetic constants to be used for cooling rate calculations are those derived from Equations 3 or 4 while, in the second case, one should use the values obtained by annealing experiments on the investigated sample, as we have here in deriving Equation 9. The problem would be even more crucial if the exsolution process and the ordering took place simultaneously. For the orthopyroxene of Johnstown diogenite, we obtained a cooling rate of 10^{-7} Ky^{-1} at T = 375 °C using Equation 9, while Zema et al. (1997) obtained a value of 0.084 Ky^{-1} using Equation 3. The difference between the two values is astonishing. Whereas the value of 10^{-7} Ky^{-1} is definitely too slow, the value of 0.084 Ky^{-1} can be considered reasonable if compared to the cooling rates obtained by Miyamoto and Takeda (1994) on a meteorite sample coming from the same parent body. This suggests that, at least for Johnstown diogenite, the ordering process did not take place after the exsolution process. However, if the value of 85 kcal/mol for the activation energy for Ca diffusion (Brady and McCallister 1983) is considered, one would expect that Ca diffusion takes place before the Fe-Mg ordering. The evident contradiction between the two models does not permit a final conclusion, for which a thorough investigation on how the exsolution mechanisms interfere with Mg-Fe diffusion in orthopyroxene would be necessary.

ACKNOWLEDGMENTS

This work was supported by the E.C. Contract N. ERBFMRX-CT97-0108 "Mineral Transformations" and by the Italian MURST Project "Relation between structure and properties in minerals: analysis and applications." We are grateful to the A.E. Kathryn Nagy, H. Kroll, and an anonymous reviewer for their critical comments and helpful suggestions.

REFERENCES CITED

Anovitz, L.M., Essene, E.J., and Dunham, W.R. (1988) Order-disorder experiments on orthopyroxenes: implications for the orthopyroxene geospeedometer. American Mineralogist, 73, 1060–1073.

Besancon, J.R. (1981) Rate of cation disordering in orthopyroxenes. American Mineralogist, 66, 965–973.

Blessing, R.H., Coppens, P., and Becker, P. (1974) Computer analysis of step-scanned X-ray data. Journal of Applied Crystallography, 7, 488–492.

Brady, J.B. and McCallister, R.H. (1983) Diffusion data for clinopyroxenes from homogenization and self-diffusion experiments. American Mineralogist, 68, 95–105.

Cannillo, E., Germani, G., and Mazzi, F. (1983) New crystallographic software for Philips PW 1100 single crystal diffractometer. CNR Centro di Studio per la Cristallografia, Internal Report 2.

Coppens, P. and Hamilton, W.C. (1970) Anisotropic extinction in the Zachariasen approximation. Acta Cristallographica, A26, 71–83.

Domeneghetti, M.C., Molin, G.M., Stimpfl, M., and Tribaudino, M. (1995) Orthopyroxene from the Serra de Magé meteorite: structure refinement and estimation of *C*2/*c* pyroxene contributions to apparent *Pbca* diffraction violations. American Mineralogist, 80, 923–929.

Domeneghetti, M.C., Tazzoli, V., Boffa Ballaran, T., and Molin, G.M. (1996) Orthopyroxene from the Serra de Magé meteorite: a structure refinement procedure for a *Pbca* phase coexisting with a *C*2/*c* exsolved phase. American Mineralogist, 81, 842–846.

Floran, R.J., Prinz, M., Hlava, P.F., Keil, K., Spettel, B., and Wänke, H. (1981) Mineralogy, petrology, and trace element geochemistry of the Johnstown meteorite: a brecciated orthopyroxenite with siderophile and REE-rich components. Geochimica et Cosmochimica Acta, 45, 2385–2391.

Fredriksson, K., Noonan, A., Brenner, P., and Sudre, C. (1976) Bulk and major phase composition of eight hyperstene achondrites. Meteoritics, 11, 278–280.

Ganguly, J. (1982) Mg-Fe order-disorder in ferromagnesian silicates II. In S.K. Saxena, Ed., Thermodynamics: Kinetics and Geological Applications, p. 58–99. Springer, Berlin.

Ganguly, J. and Domeneghetti, M.C. (1996) Cation ordering of orthopyroxenes from the Skaergaard Intrusion: implications for the subsolidus cooling rates and permeabilities. Contributions to Mineralogy and Petrology, 122, 359–367.

Ganguly, J. and Tazzoli, V. (1994) Fe^{2+}-Mg interdiffusion in orthopyroxene: Retrieval from data on intracrystalline exchange reaction. American Mineralogist, 79, 930–937.

Ganguly, J., Yang, H., and Ghose, S. (1994) Thermal history of mesosiderites: quantitative constraints from compositional zoning and Fe-Mg ordering in orthopyroxenes. Geochimica et Cosmochimica Acta, 58, 2711–2723.

Kroll, H., Lueder, T., Schlenz, H., Kirfel, A., and Vad, T. (1997) The Fe^{2+},Mg distribution in orthopyroxene: A critical assessment of its potential as a geospeedometer. European Journal of Mineralogy, 9, 705–733.

Ibers, J.A. and Hamilton, W.C., eds. (1974) International Tables for X-ray Crystallography, vol. 4. p. 99–101. Kynoch Press, Birmingham, U.K.

James, F. and Roos, M. (1975) MINUIT, a system for function minimisation and analysis of the parameter errors and correlations. CERN/DD, Internal Report 75/20, Computational Physics, 10, 343–347.

Lehmann, M.S. and Larsen, F.K. (1974) A method for location of the peaks in step-scan measured Bragg reflections. Acta Crystallographica, A30, 580–584.

Mittlefehldt, D.W. (1994) The genesis of diogenites and HED parent body petrogenesis. Geochimica et Cosmochimica Acta, 58, 1537–1552.

Miyamoto, M. and Takeda, H. (1994) Cooling rates of several cumulate eucrites. Meteoritics, 29, 505–506.

Molin, G.M., Saxena, S.K., and Brizi, E. (1991) Iron-magnesium order-disorder in an orthopyroxene crystal from the Johnstown meteorite. Earth and Planetary Science Letters, 105, 260–265.

Molin, G.M., Domeneghetti, M.C., Salviulo, G., Stimpfl, M., and Tribaudino, M. (1994) Antarctic FRO90011 lodranite: cooling history from pyroxene crystal chemistry and microstructure. Earth and Planetary Science Letters, 128, 479–487.

Mori, H. and Takeda, H. (1981) Thermal and deformational histories of diogenites as inferred from their microtextures of orthopyroxene. Earth and Planetary Science Letters, 53, 266–274.

Mueller, R.F. (1967) Model for order-disorder kinetics in certain quasi-binary crystals of continuously variable composition. Journal of Physics and Chemistry of Solids, 28, 2239–2243.

——(1969) Kinetics and thermodynamics of intracrystalline distribution. Mineralogical Society American Special Paper, 2, 83–93.

North, A.C.T., Phillips, D.C., and Mathews, F.S. (1968) A semi-empirical method of absorption correction. Acta Crystallographica, A24, 351–359.

Rossi, G., Smith, D.C., Ungaretti, L., and Domeneghetti, M.C. (1983) Crystal-chemistry and cation ordering in the system diopside-jadeite: a detailed study by crystal structure refinement. Contribution to Mineralogy and Petrology 83, 247–258.

Saxena, S.K. and Ghose, S. (1971) Mg^{2+}-Fe^{2+} order-disorder and thermodynamics of the orthopyroxene-crystalline solution. American Mineralogist, 56, 532–559.

Saxena, S.K., Tazzoli, V., and Domeneghetti, M.C. (1987) Kinetics of Fe^{2+}-Mg dis-

tribution in aluminous orthopyroxenes. Physics and Chemistry of Minerals, 15, 140–147.

Saxena, S.K., Domeneghetti, M.C., Molin, G.M., and Tazzoli, V. (1989) X-ray diffraction study of Fe^{2+}-Mg order-disorder in orthopyroxene. Some kinetic results. Physics and Chemistry of Minerals, 16, 421–427.

Seifert, F. (1983) Mössbauer line broadening in aluminous orthopyroxenes: evidence for next nearest neighbors interactions and short-range order. Neues Jahrbuch für Mineralogie Abhandlungen, 148, 141–162.

Sheldrick, G.M. (1993) SHELXL-93, A program for crystal structure refinement, University of Goettingen, Germany.

Skogby, H. (1992) Order-disorder kinetics in orthopyroxenes of ophiolite origin. Contributions to Mineralogy and Petrology, 109, 471–478.

Stimpfl, M., Ganguly, J., and Molin G.M. (1999) Fe^{2+}-Mg order-disorder in orthopyroxene: Equilibrium fractionation between the octahedral sites and thermodynamic analysis. Contributions to Mineralogy and Petrology, in press.

Sykes-Nord, J.A. and Molin, G.M. (1993) Mg-Fe order-disorder reaction in Fe-rich orthopyroxene: structural variation and kinetics. American Mineralogist, 78, 921–931.

Tokonami, M. (1965) Atomic scattering factors for O^{2-}. Acta Crystallographica, 19, 486.

Yang, H. and Ghose, S. (1994) In situ Fe-Mg order-disorder studies and thermodynamic properties of orthopyroxenes $(Fe,Mg)_2Si_2O_6$. American Mineralogist, 79, 633–643.

Zema, M., Domeneghetti, M.C., and Molin, G.M. (1996) Thermal history of Acapulco and ALHA81261 acapulcoites constrained by Fe^{2+}-Mg ordering in orthopyroxene. Earth and Planetary Science Letters, 144, 359–367.

Zema, M., Domeneghetti, M.C., Molin, G.M., and Tazzoli, V. (1997) Cooling rates of diogenites: a study of Fe^{2+}-Mg ordering in orthopyroxene by single-crystal x-ray diffraction. Meteoritics and Planetary Science, 32, 855–862.

Zema, M., Domeneghetti, M.C., Molin, G.M. and Tazzoli, V. (1999) Do exsolutions influence the kinetics of the order-disorder reaction in orthopyroxene? Phase Transition, 69, 35–46s.

MANUSCRIPT RECEIVED DECEMBER 29, 1998
MANUSCRIPT ACCEPTED JULY 12, 1999
PAPER HANDLED BY KATHRYN L. NAGY